ACS APPLIED MATERIALS & INTERFACES

www.acsami.org

Research Article

Surface Defect Engineering of MoS_2 for Atomic Layer Deposition of TiO_2 Films

Jaron A. Kropp, Ankit Sharma, Wenjuan Zhu, Can Ataca,* and Theodosia Gougousi*

Cite This: *ACS Appl. Mater. Interfaces* 2020, 12, 48150–48160

Read Online

ACCESS | Metrics & More | Article Recommendations | Supporting Information

ABSTRACT: In this manuscript, we combine experimental and computational approaches to study the atomic layer deposition (ALD) of dielectrics on MoS_2 surfaces for a very common class of ALD precursors, the alkylamines. More specifically, we study the thermal ALD of TiO_2 from TDMAT and H_2O. Depositions on as-produced chemical vapor deposition MoS_2 flakes result in discontinuous films. Surface treatment with mercaptoethanol (ME) does not improve the surface coverage, and DFT calculations show that ME reacts very weakly with the MoS_2 surface. However, creation of sulfur vacancies on the MoS_2 surface using Ar ion beam irradiation results in much improved surface coverage for films with a nominal thickness of 6 nm, and the calculations show that TDMAT reacts moderately with either single or extended sulfur vacancies. ME also reacts with the vacancies, and defect-rich surfaces treated with ME provide an equally good surface for the nucleation of ALD TiO_2 films. The computational studies however reveal that the creation of surface vacancies results in the introduction of gap states that may deteriorate the electronic properties of the stack. Treatment with ME results in the complete removal of the gap states originating from the most commonly found single vacancies and reduces substantially the density of states for double and line vacancies. As a result, we provide a pathway for the deposition of high-quality ALD dielectrics on the MoS_2 surfaces, which is required for the successful integration of these 2D materials in functional devices.

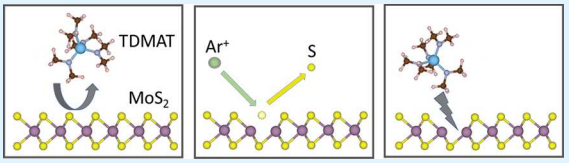

KEYWORDS: *molybdenum disulfide, atomic layer deposition, sulfur vacancy, TDMAT, density functional theory*

INTRODUCTION

Monolayer molybdenum disulfide (MoS_2) is a two-dimensional (2D) semiconductor material that primarily exists in a hexagonal structure (2H-MoS_2). Monolayer 2H-MoS_2 possesses a direct band gap of ∼1.8 eV and is therefore of interest for electronic, optoelectronic, and sensing applications.[1,2] Recently, chemical vapor deposition (CVD) methods have been developed to grow high-quality, large-area single-crystal MoS_2 monolayers.[3−7] If these MoS_2 monolayers are to be used in a device such as a field-effect transistor, they need to be integrated with a high-quality dielectric material. Atomic layer deposition (ALD) has been used extensively to deposit high-k dielectric films on mainstream semiconductors because of the high film quality, purity, and the ability to coat nonplanar geometries. For ALD of metal oxide films, a hydrophilic surface is required.[8] This is usually accomplished by preparing the starting surface with an −OH termination, which is fairly straightforward for surfaces covered with an oxide layer. The MoS_2 surface, however, is inert and hydrophobic. A prime example of ALD of metal oxides on inert, hydrophobic surfaces is the hydrogen-terminated Si (Si-H) surface that has been studied extensively. For Si-H surfaces in general, it is known that film formation occurs on defect sites. The Si-H surface is unstable at normal processing temperatures leading to the progressive increase of the defect density and eventually the formation of continuous films after what is known as an incubation period.[9] Like Si-H, the MoS_2 surface is inert and hydrophobic, but unlike Si-H, it is stable at normal processing temperatures and, as a result, not an ideal starting surface for the ALD of metal oxide films. Typical MoS_2 surfaces contain up to ∼10% sulfur vacancies, which are more reactive than the pristine surface and may serve as nucleation sites for ALD films.[10] However, at this concentration, the defects are not sufficient to produce continuous coverage even for films several nanometers in thickness. As a result, the creation of higher defect density or the introduction of an anchor species on the surface is required to seed growth. Such a molecule should have two different end groups: one that would interact with the −S surface termination and −OH termination on the opposite side to seed film growth. There are examples where one of these approaches has been used to achieve uniform, pinhole-free films on MoS_2.[11−22]

In this work, we investigate the effect of sulfur vacancies on the surface coverage obtained for a typical ALD process by using Ar ion sputtering to control their density. While defect creation may increase the reactivity of the MoS_2 surface, density functional theory (DFT) calculations of the electronic

Received: July 20, 2020
Accepted: September 24, 2020
Published: September 24, 2020

https://dx.doi.org/10.1021/acsami.0c13095
ACS Appl. Mater. Interfaces 2020, 12, 48150–48160

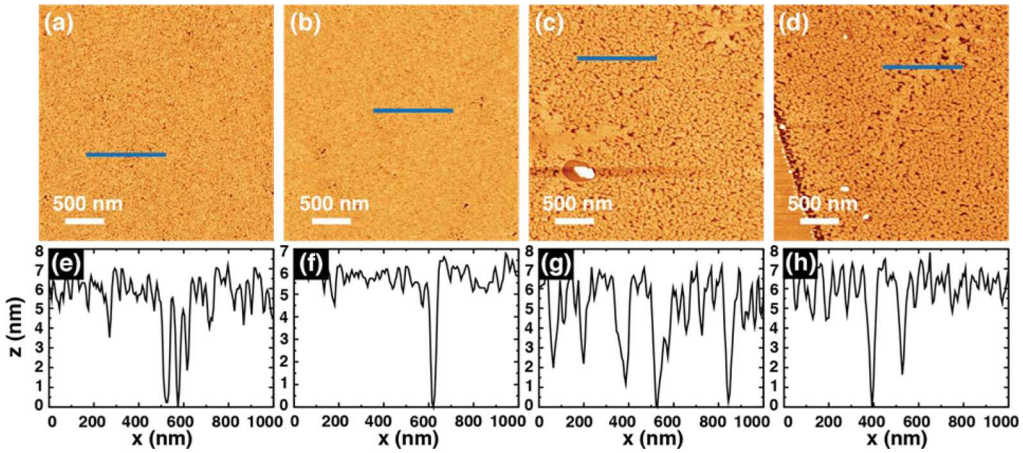

Figure 1. AFM images of 6 nm TiO_2 deposited on (a, b) untreated MoS_2 and (c, d) MoS_2 treated with mercaptoethanol. Blue bars mark the location of line profiles shown below each image in (e, f) for untreated MoS_2 and (g, h) for treated MoS_2.

band structure show that such vacancies introduce localized states into the band gap. We therefore investigate the effectiveness mercaptoethanol (ME) as a seed for the ALD of TiO_2 both on as-received and argon ion-treated CVD MoS_2 surfaces. Mercaptoethanol ($HOCH_2CH_2SH$) is a short thiol with an −SH group at the tail and is hydroxyl (−OH) terminated on its other end, and thus, it meets the anchor molecule requirement stated before. Thiols are known to interact with the naturally occurring vacancies and may be used to heal the vacancies and restore the electronic properties of the MoS_2 surface.[20,23−28,21,29−34] The experimental work is complemented by calculations of the energetics of thiol and ALD precursor adsorption on pristine and vacancy-containing MoS_2 surfaces using density functional theory. This combined approach provides significant insights into the mechanism of ALD film growth on MoS_2.

RESULTS

Atomic Layer Deposition of TiO_2 on MoS_2. Deposition of TiO_2 films on untreated MoS_2 monolayers results in noncontinuous films that contain many pinholes. As an example, Figure 1a,b shows AFM images of 6 nm TiO_2 deposited on MoS_2 at 100 °C. AFM line profiles measure the depth of the pinholes as ∼6 nm. MoS_2 surfaces are hydrophobic, so it is not surprising that the ALD process fails to provide continuous coverage. This also demonstrates the need to alter the surface energy to promote film nucleation. ME is a thiol with an −OH group on the opposite end, and we hypothesize that the presence of this group on the surface would provide more film nucleation sites. However, depositions of 6 nm films on ME-treated surfaces (Figure 1c,d) result in films that contain wider pinholes and on average show decreased surface coverage than films on the untreated surfaces.

We use DFT calculation to study the interaction of ME with various MoS_2 surfaces (Figure S1, Table S1), and we find that the ME interacts only weakly with pristine surfaces but more strongly with sulfur vacancies. Clearly, the results in Figure 1c,d show that the natural abundance of defects on the MoS_2 surface is not high enough to result in continuous film coverage. To create a higher concentration of reactive defect sites, we sputter the MoS_2 monolayers with argon ions. Analysis of the XPS results shows that the as-grown CVD MoS_2 surface contains ∼5% vacancy sites, which includes possible defects present on both sides of the monolayer. The evolution of the surface defect density as a function of the sputter time and ion fluence is shown in Figure 2. Sputtering

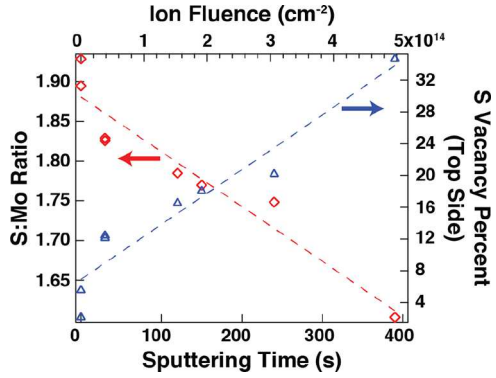

Figure 2. Left axis (red line) plots the sulfur:molybdenum ratio of MoS_2 as a function of sputter time/ion fluence as calculated from XPS peak fitting. The right axis (blue line) plots the calculated sulfur vacancy percentage on the top side as a function of the sputter time/ion fluence. Multiple data points at 0 and 30 s correspond to measurements taken on two separate samples.

for 390 s (corresponding to an ion fluence of $F = 4.97 \times 10^{14}$ cm^{-2}) generates up to 35% sulfur vacancies on the top side. The shortest sputter duration, 30 s ($F = 3.83 \times 10^{13}$ cm^{-2}), generates ∼10% sulfur vacancies. It is expected that the vacancies generated by sputtering are on the top side of the MoS_2 surface only as a consequence of the sample geometry.

Ion bombardment is a highly invasive surface treatment, so it is important to consider its effect on the surface structure. Argon plasma has been shown to induce a phase change in MoS_2, and the change from the 2H phase to the 1T phase is detectable with XPS analysis.[35] High-resolution XP spectra of the Mo 3d and S 2p regions (Figure 3) taken before and after ion sputtering show little change in the peak shape. This confirms that the treatment did not induce phase changes or destroy the MoS_2 layer but preferentially creates sulfur vacancies on an otherwise intact 2H-MoS_2 surface.

The sputtered MoS_2 samples (up to 390 s, ∼35% S vacancies) are treated with mercaptoethanol vapor before subsequent ALD of 6 nm TiO_2. As a control, we also perform ALD on sputtered samples with no thiol treatment. AFM

https://dx.doi.org/10.1021/acsami.0c13095
ACS Appl. Mater. Interfaces 2020, 12, 48150−48160

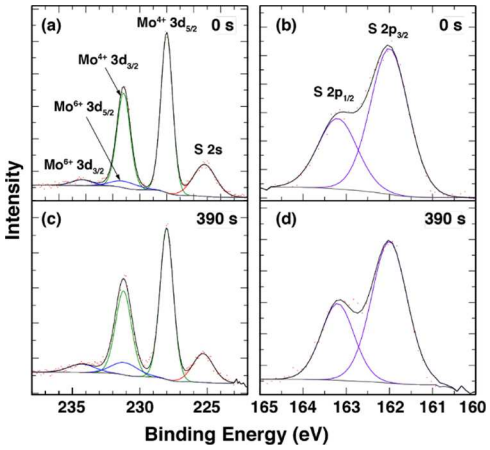

Figure 3. X-ray photoelectron spectra of the (a) Mo 3d region (no sputtering) and (b) S 2p region (no sputtering) as well as the (c) Mo 3d region (390 s sputtering) and (d) S 2p region (390 s sputtering).

characterization of the surface morphology of TiO_2 films on sputtered, ME-treated MoS_2 samples reveals films that are uniform and pinhole-free (Figure 4a–c). TiO_2 films on the control MoS_2 samples are similarly uniform and free of pinholes (Figure 4g–i). This suggests that the increased concentration of sulfur vacancies alone, as compared to as-grown CVD MoS_2, is sufficient to promote smooth, conformal, and coalesced ALD film growth. Both sets of samples exhibit dendritic structures on the surface that are ~1 nm in height.

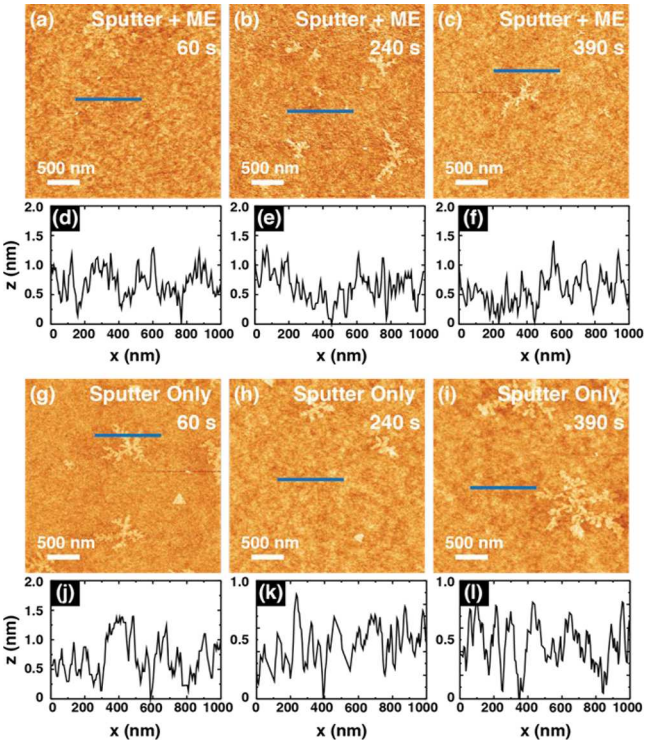

Figure 4. AFM images of 6 nm TiO_2 deposited on ME-treated MoS_2 that was sputtered for (a) 60 s, (b), 240 s, and (c) 390 s. Line profiles marked by the blue bars are shown for sputter times of (d) 60 s, (e), 240 s, and (f) 390 s. Also shown are AFM images of 6 nm TiO_2 deposited on untreated MoS_2 that was sputtered for (g) 60 s, (h) 240 s, and (i) 390 s with corresponding line profiles shown in (j), (k), and (l).

Similar features have been observed in thermally oxidized MoS_2, and it is possible that these dendrites are formed by the oxidation of the defective MoS_2 layer.[36]

O_2, H_2O, and TDMAT Adsorption on Bare MoS_2 and S Vacancies. Motivated by the observation of uniform film growth on the untreated 10–35% vacancy-containing MoS_2 (Figure 4g–i), we calculate the adsorption energies of O_2, H_2O, and TDMAT molecules on the pristine and single-S vacancy sites. We consider O_2 and H_2O molecules as possible seed molecules for TiO_2 film growth as they are abundant in air and may react with TDMAT to form TiO_2.[37,38] It has been reported in literature that O_2 and H_2O do not bind strongly with the pristine MoS_2 surface.[39,40] The final geometry and adsorption energy for these molecules on the S vacancy are shown in Figure 5. Calculation parameters and simulation

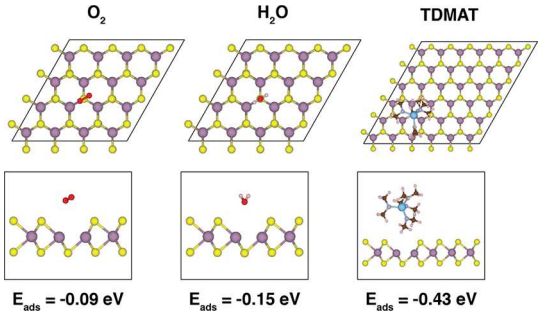

Figure 5. Adsorption geometries and energies of O_2, H_2O, and TDMAT on a single-S vacancy. The atoms shown in the figure are as follows: Mo (purple), S (yellow), O (red), C (brown), H (white), N (pale blue), and Ti (bright blue).

details can be found in the "Computational Methods" section. The adsorption energy of TDMAT on MoS_2 is calculated in a $6 \times 6 \times 1$ supercell to avoid interactions between the relatively large TDMAT molecule and its periodic images. In agreement with previous works, we find that O_2 and H_2O adsorb weakly above the S vacancy.[41,42] TDMAT binds most strongly of all molecules considered here, with an adsorption energy of −0.43 eV. On the pristine MoS_2 surface, TDMAT adsorbs with an energy of −0.23 eV. Similar calculations for the interaction of ME with the MoS_2 surfaces are shown in the Supporting Information.

Adsorption on Extended Defects. Because of the high concentration of defects on our sputtered MoS_2 surfaces, it is likely that extended defects are present. Cluster expansion is used to generate structures with the desired sulfur vacancy concentration (0–40%) and identify the most favorable arrangement of the vacancies (Figure S2). The cluster expansion calculations reveal that, in addition to single-sulfur vacancies, extended line defects of missing sulfur atoms are favorable at these defect concentrations (Figure S3). Thus, we investigate the adsorption of the above-mentioned species and ME on both an extended line defect and a simpler double-sulfur (S_2) vacancy. ME physisorbs above the S_2 vacancy with an energy of −0.25 eV, which is similar to the adsorption energy on a single-S vacancy. Once trapped in the physisorption well, there is a very small thermal barrier (0.09 eV) to transition to the chemisorbed state where it is strongly bound (E_{ads} = −2.43 eV). The energetics of this process are shown in Figure 6. In the resulting geometry, the S–H bond is broken, and the thiol chain passivates one-sulfur vacancy site while the H atom bonds in the neighboring site. The thiol

https://dx.doi.org/10.1021/acsami.0c13095
ACS Appl. Mater. Interfaces 2020, 12, 48150–48160

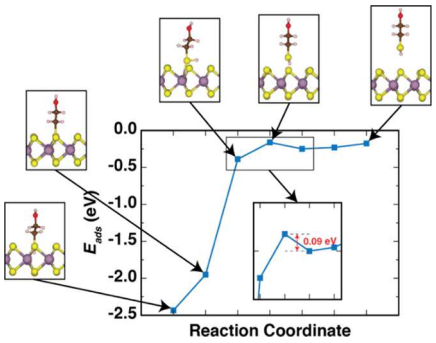

Figure 6. Energy barrier calculations of the ME molecule in a sulfur-double vacancy. The inset shows the barrier measured at ∼0.09 eV. The atoms shown in the figure are as follows: Mo (purple), S (yellow), O (red), C (brown), and H (white)

chain binds with energy −1.39 eV and remains chemisorbed in the vacancy after 1 ps of AIMD simulations at 600 K, indicating that this system is dynamically stable. These results show similarities with the single-S vacancy, but the energy barrier for the ME molecule to bind inside the vacancy is reduced significantly. The adsorption energetics of O_2, H_2O, and TDMAT on the S_2 vacancy are similar to the single-vacancy case. In contrast, the physisorption of these molecules on extended line vacancies is stronger than with either the single-S or S_2 vacancies. The adsorption energies are compiled in Table 1.

We further investigate the chemisorption and dissociation of O_2 and H_2O on vacancy defects, as O_2 dissociation on the single-S vacancy has previously been found to be favorable.[43,44] The O_2 molecule may chemisorb in the S_2 vacancy by overcoming an energy barrier of ∼0.1 eV, and the resulting adsorption energy is E_{ads} = −2.30 eV (see Figure S4e). Furthermore, dissociation of the O_2 molecule in the S_2 vacancy is energetically most favorable and results in E_{ads} = −7.94 eV. The resulting configuration in this case is that each oxygen atom occupies neighboring S vacancy sites (Figure S4f).

Since previous works have shown that the O_2 molecule may dissociate on the S vacancy leaving one oxygen atom adsorbed

Table 1. Adsorption Energies of Mercaptoethanol, TDMAT, O_2, and H_2O on MoS_2 Surfaces. The Surfaces Considered Are Pristine MoS_2 (Figure S4a), MoS_2 with a Single-S Vacancy (Figure S4b), MoS_2 with a Double-S Vacancy (S_2 Vacancy, Figure S4c), and MoS_2 with a Line Vacancy (Figure S4d)

Surface	Molecule	Adsorption Energy on Site (eV)			
Pristine MoS_2 (Figure S4a)		Top S	Top Mo	Bridge	Hollow
	Mercaptoethanol	-0.15	-0.18	-0.14	-0.17
	TDMAT	-0.22	-	-	-
	O_2	-0.02	-	-	-
	H_2O	-0.04	-	-	-
MoS_2 Single S Vacancy (Figure S4b)		Top S Vacancy (Physisorbed)	In S Vacancy (Chemisorbed)		
	Mercaptoethanol	-0.27	-0.25		
	TDMAT	-0.43	-		
	O_2	-0.10	-2.13		
	H_2O	-0.15	-		
MoS_2 Double S Vacancy (Figure S4c)		Top S Vacancy (Physisorbed)	In S Vacancy (Chemisorbed)	In S Vacancy (dissociated)	
	Mercaptoethanol	-0.25	-2.43 -1.39 (thiol chain)	-	
	TDMAT	-0.46	-	-	
	O_2	-0.08	-2.30	-7.94	
	H_2O	-0.15	-	-	
MoS_2 Line Vacancy (Figure S4d)		Top Vacancy (Physisorbed)	In Vacancy (Chemisorbed)	In S Vacancy (dissociated)	
	Mercaptoethanol	-0.69	-2.67	-	
	TDMAT	-0.86	-	-	
	O_2	-0.19	-1.69	-7.73	
	H_2O	-0.62	-0.86		

https://dx.doi.org/10.1021/acsami.0c13095
ACS Appl. Mater. Interfaces 2020, 12, 48150−48160

Table 2. Adsorption Energies of Mercaptoethanol and TDMAT on O_2-MoS_2 Surfaces. The Surfaces Considered Are an S_2 Vacancy with a Chemisorbed O_2 Molecule (Figure S4e), an S_2 Vacancy with Substitutional Oxygen Resulting from O_2 Dissociation (Figure S4f), and "Functionalized" Surfaces whereby One Oxygen Atom Adsorbs on the Surface after Dissociation (Figure S4g,h)

Surface	Molecule	Adsorption Energy on Site (eV)	
MoS_2 S_2 Vacancy-O_2 Molecule (Figure S4e)		Top O_2	
	Mercaptoethanol	-0.15	
	TDMAT	-0.39	
MoS_2 S_2 Vacancy-O_2 Substitution (Figure S4f)		Top O	Bridge
	Mercaptoethanol	-0.28	-0.29
	TDMAT	-0.45	-
MoS_2 S Vacancy-O Functionalized (Figure S4g)		Top Substitutional O	On Adsorbed O
	Mercaptoethanol	-0.37	-0.07
	TDMAT	-	-0.17
MoS_2 S_2 Vacancy-O Functionalized (Figure S4h)		Top Substitutional O	On Adsorbed O
	Mercaptoethanol	-0.34	-0.07
	TDMAT	-	-0.24

on the surface,[43,44] we calculate the energy of similar configurations on both single-S (Figure S4g) and double-S_2 (Figure S4h) vacancies. These "functionalized" cases result in E_{ads} = −4.65 eV and E_{ads} = −4.12 eV for S and S_2 vacancies, respectively. Unlike the O_2 molecule, the H_2O molecule does not chemisorb in the double vacancy but remains physisorbed on the surface.

Since the chemisorption of oxygen in extended sulfur vacancies is likely, we investigate further the adsorption of ME and TDMAT molecules on these oxygen-containing MoS_2 surfaces (Table 2). First, we consider the case of the O_2 molecule chemisorbed in the S_2 vacancy (Figure S4e). The ME interaction with this system is weak, with E_{ads} = −0.15 eV, but TDMAT can adsorb with E_{ads} = −0.39 eV. Next, we consider adsorption on the dissociated O_2 molecule in the S_2 vacancy. Here, ME may adsorb with E_{ads} = −0.28 eV, which is comparable to the adsorption energy of ME on an unpassivated single-S vacancy. TDMAT adsorbs with E_{ads} = −0.45 eV, which is again comparable to its interaction with a single-S vacancy. We can conclude that oxygen chemisorption on the defective MoS_2 surface has minor effects (either none or slightly lowering the adsorption energy) on the adsorption of ME and TDMAT. Similar binding trends are calculated for extended line vacancy defects (Table 1).

Electronic Structure. To investigate the utility of defective and functionalized MoS_2 for electronic devices, we calculate the band structures and density of states of pristine, defective, and thiol-functionalized MoS_2 monolayers using DFT. The band gap of pristine MoS_2 calculated in the generalized gradient approximation is 1.62 eV (Figure 7a), in good agreement with previously published works.[45,46] Although GGA is known to underestimate the true band gap, trends in changes to the band gap are preserved. To study the effects of S vacancies on the electronic structure, we compare the density of states of pristine and vacancy-containing MoS_2 with and without ME adsorption. A single-isolated vacancy introduces a localized state below the conduction band (Figure 7b). The double-sulfur vacancy introduces several states below the conduction band (Figure 7c), while the extended line vacancy results in a drastically altered band structure where the band gap is reduced to 0.37 eV (Figure 7d). ME adsorption on the pristine surface does not alter the electronic properties significantly (Figure 7e), but Figure 7f shows that ME chemisorbed in a single-sulfur vacancy removes the gap state and completely passivates the vacancy. However, ME bonding to the double (Figure 7g) or line vacancy (Figure 7h) cannot fully passivate the vacancy and does not remove the gap states.

Our DFT results indicate that oxygen adsorption on sulfur vacancies is energetically favorable. Investigation of the electronic properties of the O_2-MoS_2 systems can therefore indicate which, if any, vacancy-containing surfaces are suitable for electronic device purposes. Oxygen interacts most easily with the S_2 vacancy. Physisorbed O_2 above the vacancy does not alter the density of states, leaving the gap states present. The O_2 molecule can overcome a small energy barrier (∼0.1 eV) to bond in the S_2 vacancy (Figure S4e). The double vacancy is not fully passivated in this state, and gap states are present below the conduction band (Figure 8a). However, the dissociation of the O_2 molecule in the S_2 vacancy results in the removal of the gap states (Figure 8b). ME adsorption on top of the chemisorbed O_2 molecule (Figure S4e) introduces a localized state at the top of the valence band (Figure 8c), and the gap states are still present. However, when ME is allowed to chemisorb in the S vacancy neighboring the O_2 molecule

https://dx.doi.org/10.1021/acsami.0c13095
ACS Appl. Mater. Interfaces 2020, 12, 48150−48160

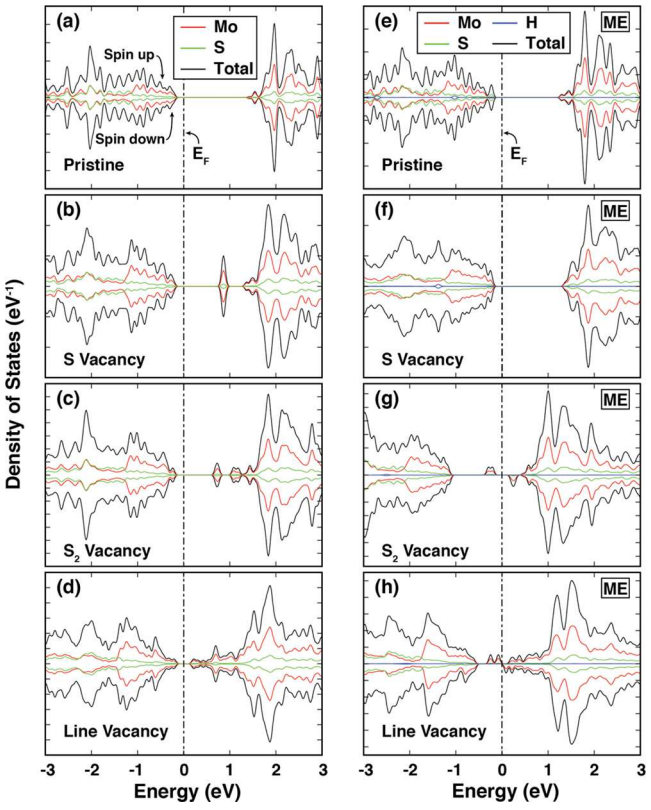

Figure 7. Spin-polarized density of states of (a) pristine MoS_2, (b) MoS_2 with a single-S vacancy, (c) MoS_2 with a double-S vacancy, and (d) MoS_2 with a line vacancy. Also shown are (e) ME on pristine MoS_2, (f) ME in a single-S vacancy, (g) ME in a double-S vacancy, and (h) ME in a line vacancy.

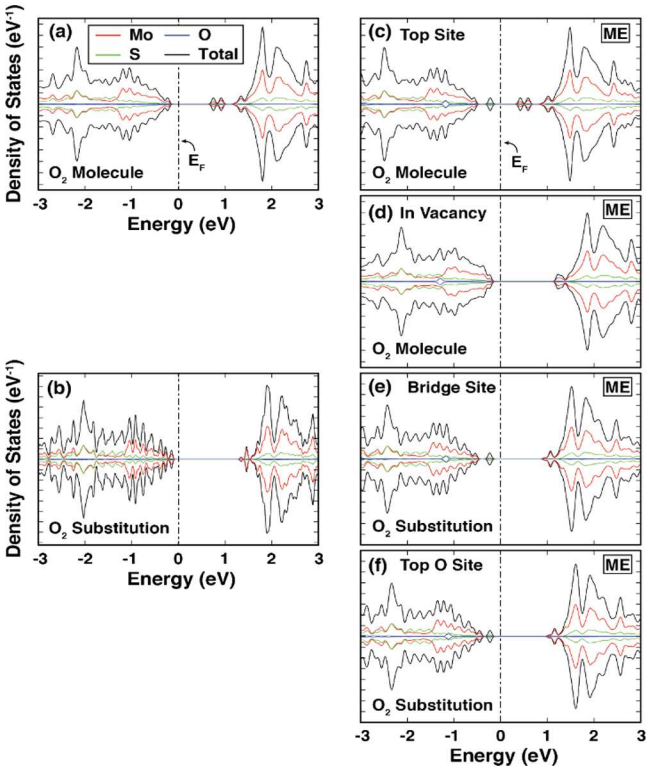

Figure 8. Spin-polarized density of states of an O_2 molecule (a) adsorbed in a double-sulfur vacancy and (b) dissociated in a double-sulfur vacancy (O atoms substitute for the missing S atoms). Also shown are the spin-polarized density of states of an ME molecule adsorbed on the O_2-MoS_2 surface on (c) the top site of O_2 and (d) the vacancy next to O_2. On the dissociated O_2 molecule, the density of states is shown for ME on (e) the bridge site between O atoms and (f) on the top site of one O atom. The ME molecule introduces a localized state just below the valence band.

(Figure S4f), both the localized valence state and gap states are removed (Figure 8d). When ME adsorbs on dissociated oxygen-MoS_2 surfaces (Figure S4g,h), a localized state is present at the top of the valence band (Figure 8e,f).

DISCUSSION

It is well known that ALD of metal oxides on pristine, untreated MoS_2 surfaces typically results in poor quality films that are not fully coalesced.[11−19] This necessitates the use of seeding approaches to modify the surface energy and consequently its reactivity. Self-assembled monolayer (SAM)-type approaches are quite popular as they rely on self-assembly that can be accomplished in exposure times ranging from a few minutes to several hours. Thiols are commonly used SAM molecules and have been used on MoS_2 surfaces as they are expected to interact with the −S terminated surface or sulfur vacancies.[20,21,23−34] One such thiol, mercaptoethanol (that has an −OH terminal group), is used in this work to promote the growth of TiO_2 ALD films on MoS_2. However, the results presented here suggest that a simple ME vapor treatment is not sufficient to improve film nucleation. DFT calculations indicate that ME adsorption on the pristine MoS_2 surface is weak. Coupled with XPS analysis of the as-received CVD MoS_2 starting surfaces that indicates a low (∼5%) concentration of sulfur defects, these facts explain the formation of non-continuous ALD films on ME-treated MoS_2. This observation points out that an increased concentration of surface defect sites may be required to achieve uniform film growth. Sputtering the MoS_2 surface with argon ions is used to produce increased concentrations (∼10−35%) of sulfur vacancies, and *in situ* XPS during ion bombardment shows that the S:Mo ratio decreases with the sputtering time (Figure 2), indicating that sulfur is preferentially removed during ion-beam irradiation. Importantly, the XPS measurements do not show any noticeable changes in peak shapes for the Mo 3d and S 2p regions (Figure 3), which indicate that the ion bombardment does not destroy the surface geometry. After treating these samples with ME, ALD of TiO_2 films results in uniform film growth, with no visible pinholes or gaps. However, sputtered samples that were not treated with ME show a very similar film morphology (Figure 4), indicating that the ALD precursors may react with the untreated defect-rich surface without the need of a seeding layer.

Possible Growth Mechanisms. Sulfur vacancies are known to be reactive and expected to be passivated with oxygen or other species.[40−44,47−52] As the samples were exposed to air for a few minutes after removal from the XPS chamber, it is conceivable that the sulfur defects have reacted with atmospheric components such as O_2 and moisture producing surface termination that may facilitate interaction with the TDMAT precursor and result in uniform film growth. We investigate several possible mechanisms for the involvement of all these species in the surface reactions of untreated, vacancy-containing MoS_2, including adsorption on sulfur vacancies. The O_2 adsorption energy on a single-S vacancy is calculated as −0.09 eV, indicating weak physisorption. It has

https://dx.doi.org/10.1021/acsami.0c13095
ACS Appl. Mater. Interfaces 2020, 12, 48150−48160

been shown previously that oxygen may chemisorb strongly in the single-S vacancy and may do so dissociatively.[41−44,49,50] However, in order for molecular oxygen to transition from the physisorbed state to the chemisorbed state in a single-S vacancy, it must overcome an energy barrier of 0.74 eV for which the transition time is estimated to be ∼20 h.[41] To reach the dissociated state where one oxygen atom fills the S vacancy and one oxygen adsorbs on a nearby S atom, another energy barrier of 0.8−0.93 eV must be overcome.[43,44] Although dissociative adsorption of O_2 would leave adsorbed oxygen atoms on the surface, which are known to seed ALD films,[12] this pathway is unlikely for single vacancies as our MoS_2 samples were exposed to air for just a few minutes at most as they were transferred from the glove box into the ALD chamber. Adsorption of H_2O is also equally unlikely (E_{ads} = −0.15 eV) on the single-S vacancy. Based on the above, we expect that single-sulfur vacancies remain unpassivated and reactive prior to thiol treatment and ALD. Conversely, the double-S_2 vacancies are more reactive to oxygen and other species. O_2 may bind strongly with a double vacancy after overcoming a small energy barrier of ∼0.1 eV. The dissociation of the O_2 molecule in the S_2 vacancy (whereby an oxygen atom is substituted in each S vacancy) is found to be energetically favorable.

Calculations of TDMAT adsorption on the single-S vacancy show that the interaction between TDMAT and the vacancy-containing MoS_2 layer is strong (E_{ads} = −0.43 eV), and AIMD simulations at 600 K do not result in desorption of the TDMAT molecule. Calculations of TDMAT adsorption on double-sulfur vacancies result in similar adsorption energies, and adsorption on line vacancies results in an even stronger interaction (E_{ads} = −0.86 eV). Therefore, TDMAT adsorption on sulfur vacancies is another possible pathway of seeding TiO_2 film growth on defect-rich MoS_2 surfaces such as those seen in Figure 4g−i. The weak interaction of O_2 and H_2O with the single-S vacancy suggests that adsorption of these molecules on single vacancies is unlikely, but adsorption of O_2 molecules on extended vacancies is expected as a result of their strong binding with double-S and line vacancies. Although oxygen may fill the extended vacancies easily, TDMAT adsorption on oxygen-containing vacancies remains strong. Thus, improved TDMAT adsorption on vacancy-containing MoS_2 is the likely mechanism behind the uniform film growth observed in Figure 4g−i.

DFT studies indicate that ME may physisorb on single-sulfur vacancies with E_{ads} = −0.25 eV, but the thiol chain can bind in a chemisorbed state (E_{ads} = −1.49 eV, Table S1). The chemisorbed thiol can seed TiO_2 film growth as it is −OH terminated and will react with TDMAT. ME is found to interact more strongly with a double vacancy or an extended line vacancy. In this case, the S−H bond is broken, the thiol chain and H atom occupy neighboring vacancies, and the thiol binds strongly (E_{ads} = −1.39 eV). AIMD indicates that this structure is stable at high temperature (600 K), and therefore, functionalization of extended vacancies with ME may be a possible pathway for the smooth film growth observed in Figure 4a−c. Likewise, ME adsorption strength is either the same or slightly lowered on O_2-MoS_2 surfaces, indicating that ME adsorption is still possible as a seed layer on these surfaces. While the presence of ME is not required for this precursor, this may not be the case for other precursor types, and as we demonstrate below, ME is required to preserve the electronic properties of the surface.

Furthermore, at the low deposition temperature used here (100 °C), some precursor condensation on the pristine surface is expected. Condensation alone is not sufficient to promote smooth film growth, as evidenced by the pinhole-containing films in Figure 1a,b, but we expect that the smooth films seen in Figure 4g−i are a result of a convolution of TDMAT condensation and TDMAT adsorption on S vacancies. This result should be applicable to all precursors of the same alkylamine family but whether it applies to other ALD precursor families should be investigated separately. Based on these results, the smooth film growth on ME-treated surfaces (Figure 4a−c) results from a combined effect of precursor condensation, TDMAT adsorption on sulfur vacancies, and TDMAT reaction with adsorbed ME or oxygen.

Electronic Properties of Defective MoS_2. While a smooth oxide layer is important for device applications, the question remains as to the usefulness of defective MoS_2 for electronic devices. DFT calculations of the electronic structure show that formation of S vacancies introduces localized states into the band gap of the MoS_2 monolayer (Figure 7b−d). These gap states can trap or scatter charge carriers and decrease the charge carrier mobility. An approach to mitigate this is required for successful device engineering. ME reacts strongly with the vacancies and provides a pathway for the removal of the gap states. However, this is possible only for single vacancies (Figure 7g,h). For extended vacancies, the adsorbed thiol molecule introduces spin-dependent gap states above and below the Fermi level. While the chemisorbed thiol chain can passivate the S vacancy that it occupies, the H atom occupying the neighboring site cannot satisfy the dangling bonds left by the absence of a sulfur atom. Likewise, O_2 and H_2O cannot fully passivate the double-S vacancy (except in the case of O_2 dissociation) and leave the system with less than desirable electronic properties. Our results suggest that there is a delicate balance between increasing surface reactivity via defect engineering and preserving the electronic properties of the channel material. ME treatment alone is not sufficient to produce smooth ALD films, and the introduction of gap states by extended vacancies cannot be mitigated by the same treatment. Therefore, the creation of vacancies should be carefully controlled as to avoid significant extended defects. It is possible that other treatments may yield improved results.

Interactions between molecular oxygen and extended sulfur vacancies are likely to occur. The calculations performed here indicate that TDMAT adsorption should not be affected by oxygen filling of sulfur vacancies, and that ME adsorption may still occur on these surfaces. While oxygen dissociation in a double-sulfur vacancy may remove the gap states and promote TDMAT adsorption, oxygen adsorption does not fully passivate the gap states without dissociation (Figure 8a,b). In the case of O_2 chemisorption, ME may still fill the second-sulfur vacancy and heal the remaining gap states. In all cases of ME adsorption on O_2-MoS_2, the ME molecule introduces a localized state just below the top of the valence band. In this situation, the band gap is not drastically altered, and so the desirable electronic properties of MoS_2 are preserved.

While perfect passivation of sulfur vacancies may not be feasible, careful engineering of the sulfur vacancy concentration along with O_2/ME saturation can restore the desired band gap properties while providing a favorable surface for TDMAT adsorption and thus TiO_2 film growth. Previous works have shown that encapsulating the MoS_2 layer with a high-k dielectric material increases charge carrier mobility,[53−55] and

https://dx.doi.org/10.1021/acsami.0c13095
ACS Appl. Mater. Interfaces 2020, 12, 48150−48160

such effects may result from O_2 saturation. Additionally, some of the damaging effects of surface vacancies may be mitigated in systems of bilayer or trilayer MoS_2, as has been reported for devices formed using plasma-enhanced ALD.[56]

CONCLUSIONS

In this manuscript, we present a combined experimental and theoretical investigation of the interaction of TDMAT with MoS_2 surfaces. We find that TDMAT interacts very weakly with the pristine MoS_2 surface resulting in films with many pinholes for nominal thickness up to 6 nm. We hypothesized that ME could be used to seed the film growth on the MoS_2 surface, but experiments showed poor surface coverage. Calculations indicated that ME interacts weakly with the MoS_2 surface but may interact more strongly with the naturally occurring sulfur vacancies. Ar ion beam irradiation was used to increase the sulfur vacancy density on the MoS_2 surface and subsequent deposition on both untreated and ME-treated samples showed complete surface coverage. The calculation indicated that TDMAT interacts directly with single- and extended-sulfur vacancies without the need for ME seeding. However, the creation of the vacancies results in the introduction of gap states that the ME treatment can passivate completely for the single vacancies and to a very large extent for the double and line vacancies. As a result, we provide a pathway for the deposition of high-quality ALD dielectrics on the MoS_2 surfaces, which is required for the successful integration of these 2D materials in functional devices.

EXPERIMENTAL METHODS

Monolayer MoS_2 samples are grown on 280 nm Si/SiO_2 substrates via CVD using solid precursors. Molybdenum trioxide (MoO_3) and sulfur (S) powder are placed into a 3″ 3-zone tube furnace in a 1:8 ratio. The substrates are suspended face-down above 0.05 g of MoO_3 using a quartz stage and placed in the center zone of the furnace. The S powder is placed in the upstream zone. The growth is conducted at atmospheric pressure, but prior to beginning the temperature ramp, 500 sccm argon is flowed as a carrier gas. The center zone is heated to 730 °C, and the upstream zone is heated to 200 °C during the growth process ramp phase. The growth lasts for ∼10 min. After the growth, the furnace is allowed to naturally cool to 50 °C before retrieving the samples. Samples are examined using an optical microscope and a Horiba Raman Confocal Imaging Microscope to confirm the presence of monolayer MoS_2.

ALD of TiO_2 films is performed at 100 °C using tetrakis dimethylamino titanium (TDMAT) and water as precursors. The deposition is performed in a custom-built ALD reactor previously described by Henegar and Gougousi.[57] Both precursors are introduced by short pulses under nitrogen flow. TDMAT and water pulses are separated by a 30 s nitrogen purge. Spectroscopic ellipsometer measurements (J.A. Woollam α-SE) performed on a companion native oxide Si(100) sample showed that the TiO_2 film thickness is ∼6.5 nm. The deposition consists of 100 ALD cycles for a nominal film thickness of 6 nm. After ALD, the TiO_2 film morphologies are analyzed via atomic force microscopy (AFM) using a Veeco Dimension 3100 AFM. The AFM images are processed using the WSXM software package.[58]

Mercaptoethanol ($SHCH_2CH_2OH$) treatment of MoS_2 samples is performed by fixing the samples to the underside of the cap of a vial containing 200 μL of pure mercaptoethanol liquid. The vials are sealed and left at room temperature for 3 h. This thiol treatment is performed in a glove box under a nitrogen atmosphere to avoid atmospheric contamination.

The MoS_2 samples are sputtered at an accelerating voltage of 700 V, and XPS data are taken *in situ* to monitor the sulfur concentration. Argon ion sputtering is performed under high vacuum at an accelerating voltage of 700 eV for 60−390 s using a Physical Electronics 04−303 differentially pumped ion gun. The sputter current is measured at ∼100 nA. The ion fluence is calculated as $F = It/qA$ where I is the sputter current, t is the sputtering time, q is the elementary electron charge, and A is the area of sputtering. X-ray photoelectron spectroscopy (XPS) data are taken *in situ* using a Kratos AXIS 165 spectrometer with an Al monochromatic X-ray source (1486.6 eV). The resulting spectra are shifted to the C 1s peak at 284.8 eV, and the S:Mo ratios R are calculated by fitting the integrated peak areas of the S 2p and Mo 3d peaks, A(S 2p) and A(Mo 3d), respectively, as

$$R = \frac{A(\text{S 2p})}{A(\text{Mo 3d})} \tag{1}$$

The peak areas are corrected for the difference in relative sensitivity factor. This ratio can be used to find the fraction of sulfur vacancies as $V_s = 1 - R/2$. Since argon ion sputtering only creates vacancies on the top side of the MoS_2 monolayer, the fraction of sulfur vacancies (considering only the top side) is doubled to $V_s = 2 - R$. However, since the as-grown MoS_2 crystal contains some natural vacancies, this expression is modified to be

$$V_s = 2 - R - V_{s,0}/2 \tag{2}$$

where $V_{s,0}$ is the naturally occurring vacancy concentration. Here, we estimate $V_{s,0} \approx 0.05$ from XPS analysis of the starting MoS_2 surfaces.

After sputtering, samples are removed from the XPS chamber under nitrogen atmosphere and sealed in vials to prevent air exposure. The vials are transferred to a nitrogen-filled glove box where select samples are treated with mercaptoethanol as described previously. The vials are resealed under an N_2 atmosphere and left for 3 h. After removal from the vials, the MoS_2 samples are transferred immediately to the ALD reactor. A control set of samples is prepared in the same manner but without the thiol vapor treatment.

COMPUTATIONAL METHODS

Density functional theory (DFT) calculations are performed using the Vienna ab initio simulation package (VASP).[59] Calculations are carried out within the generalized gradient approximation (GGA) of Perdew−Burke−Ernzerhof (PBE).[60] A cutoff energy of 520 eV and a total energy convergence of 10^{-5} eV are used for all calculations. Sulfur vacancy concentrations are adjusted by placing a single vacancy in a 2 × 2 × 1, 3 × 3 × 1, or 4 × 4 × 1 supercell corresponding to vacancy concentrations (on the top side) of 25, 11, and 6%, respectively. K-points are generated in a gamma-centered mesh of 9 × 9 × 1, 6 × 6 × 1, or 5 × 5 × 1 for the 2 × 2 × 1, 3 × 3 × 1 or 4 × 4 × 1 supercells, respectively. Double-sulfur vacancies are calculated in 6 × 6 × 1 supercells with a k-point mesh of 3 × 3 × 1, and line vacancies are calculated in rectangular 4 × 4 × 1 supercells with a k-point mesh of 3 × 5 × 1. All calculations include spin-polarization effects. Calculations of the adsorption energy of molecules on the MoS_2 surface are performed by placing the molecule ∼2 Å above the MoS_2 layer and allowing the system to relax. The adsorption energy of a molecule on the surface or sulfur vacancy is calculated as

$$E_{ads} = E(\text{Mol} + MoS_2) - E(\text{Mol}) - E(MoS_2) \tag{3}$$

where E(Mol + MoS_2) is the total energy of the combined system, E(Mol) is the total energy of the isolated molecule, and E(MoS_2) is the total energy of the isolated MoS_2 layer. The energy barrier for ME, H_2O, or O_2 molecules binding to a sulfur double vacancy in MoS_2 is calculated by fixing the molecule between 3 Å and 0 Å above the surface at 0.5 Å intervals. At each interval, only one atom in the molecule was fixed and all other atoms are allowed to relax fully. In these calculations, one Mo atom in the MoS_2 layer is fixed to prevent translation (in the vacuum direction) of the layer. When the molecule is placed in the vacancy, all atoms are allowed to relax.

Ab initio molecular dynamics (AIMD) simulations are performed using VASP to determine the dynamical stability of several molecule-MoS_2 systems. The simulations are performed at a temperature of 600 K with a timestep of 0.5 fs and run for 2000 steps (1 ps total) using

https://dx.doi.org/10.1021/acsami.0c13095
ACS Appl. Mater. Interfaces 2020, 12, 48150−48160

the Nosé-Hoover[61,62] thermostat to obtain the canonical (NVT) ensemble.

The cluster expansion method implemented using the alloy theoretic automated toolkit (ATAT)[63] is used to generate MoS_2 structures containing sulfur vacancies in concentrations from 0 to 100 percent (on a single side). The results from the cluster expansion are used to find the most energetically favorable vacancy-containing structures at the desired concentrations of ∼10−40%. Further details of the simulations are included in the Supporting Information, and the energetics of all structures are shown in Figure S1.

■ ASSOCIATED CONTENT

Supporting Information

The Supporting Information is available free of charge at https://pubs.acs.org/doi/10.1021/acsami.0c13095.

Cluster expansion calculations and example images of vacancy-containing MoS_2 structures generated by cluster expansion and images of MoS_2 and O_2-MoS_2 surfaces used in simulations of molecule adsorption and the description and energetics of ME adsorption on bare MoS_2 and S vacancies (PDF)

■ AUTHOR INFORMATION

Corresponding Authors

Can Ataca − *Department of Physics, UMBC, Baltimore, Maryland 21250, United States;* orcid.org/0000-0003-4959-1334; Email: ataca@umbc.edu

Theodosia Gougousi − *Department of Physics, UMBC, Baltimore, Maryland 21250, United States;* Email: gougousi@umbc.edu

Authors

Jaron A. Kropp − *Department of Physics, UMBC, Baltimore, Maryland 21250, United States*

Ankit Sharma − *Department of Electrical and Computer Engineering, University of Illinois at Urbana-Champaign, Urbana, Illinois 61801, United States*

Wenjuan Zhu − *Department of Electrical and Computer Engineering, University of Illinois at Urbana-Champaign, Urbana, Illinois 61801, United States;* orcid.org/0000-0003-2824-1386

Complete contact information is available at: https://pubs.acs.org/10.1021/acsami.0c13095

Author Contributions

The manuscript was written through contributions of all authors. All authors have given approval to the final version of the manuscript.

Funding

J.A.K. and T.G. acknowledge support from the National Science Foundation under grant ECCS-1407677. J.A.K. acknowledges the support of the Department of Education through a GAANN Fellowship under award number P200A150003-17. A.S. and W.Z. acknowledge support from the Office of Naval Research (ONR) under grant NAVY N00014-17-1-2973.

Notes

The authors declare no competing financial interest.

■ ACKNOWLEDGMENTS

Density functional theory calculations were performed in part at the UMBC High Performance Computing Facility (HPCF).

■ REFERENCES

(1) Mak, K. F.; Lee, C.; Hone, J.; Shan, J.; Heinz, T. F. Atomically Thin MoS_2: A New Direct-Gap Semiconductor. *Phys. Rev. Lett.* **2010**, *105*, 136805.

(2) Mak, K. F.; Shan, J. Photonics and Optoelectronics of 2D Semiconductor Transition Metal Dichalcogenides. *Nat. Photonics* **2016**, *10*, 216−226.

(3) Lee, Y.-H.; Zhang, X.-Q.; Zhang, W.; Chang, M.-T.; Lin, C.-T.; Chang, K.-D.; Yu, Y.-C.; Wang, J. T.-W.; Chang, C.-S.; Li, L.-J.; Lin, T.-W. Synthesis of Large-Area MoS_2 Atomic Layers with Chemical Vapor Deposition. *Adv. Mater.* **2012**, *24*, 2320−2325.

(4) Liu, K.-K.; Zhang, W.; Lee, Y.-H.; Lin, Y.-C.; Chang, M.-T.; Su, C.-Y.; Chang, C.-S.; Li, H.; Shi, Y.; Zhang, H.; Lai, C.-S.; Li, L.-J. Growth of Large-Area and Highly Crystalline MoS2 Thin Layers on Insulating Substrates. *Nano Lett.* **2012**, *12*, 1538−1544.

(5) Najmaei, S.; Liu, Z.; Zhou, W.; Zou, X.; Shi, G.; Lei, S.; Yakobson, B. I.; Idrobo, J.-C.; Ajayan, P. M.; Lou, J. Vapour Phase Growth and Grain Boundary Structure of Molybdenum Disulphide Atomic Layers. *Nat. Mater.* **2013**, *12*, 754−759.

(6) Zhan, Y.; Liu, Z.; Najmaei, S.; Ajayan, P. M.; Lou, J. Large-Area Vapor-Phase Growth and Characterization of MoS_2 Atomic Layers on a SiO_2 Substrate. *Small* **2012**, *8*, 966−971.

(7) Dumcenco, D.; Ovchinnikov, D.; Marinov, K.; Lazić, P.; Gibertini, M.; Marzari, N.; Sanchez, O. L.; Kung, Y.-C.; Krasnozhon, D.; Chen, M.-W.; Bertolazzi, S.; Gillet, P.; Fontcuberta i Morral, A.; Radenovic, A.; Kis, A. Large-Area Epitaxial Monolayer MoS2. *ACS Nano* **2015**, *9*, 4611−4620.

(8) Chen, R.; Kim, H.; McIntyre, P. C.; Bent, S. F. Investigation of Self-Assembled Monolayer Resists for Hafnium Dioxide Atomic Layer Deposition. *Chem. Mater.* **2005**, *17*, 536−544.

(9) Hackley, J. C.; Demaree, J. D.; Gougousi, T. Growth and Interface of HfO_2 Films on H-Terminated Si from a TDMAH and H_2O Atomic Layer Deposition Process. *J. Vac. Sci. Technol., A* **2008**, *26*, 1235−1240.

(10) Addou, R.; Colombo, L.; Wallace, R. M. Surface Defects on Natural MoS_2. *ACS Appl. Mater. Interfaces* **2015**, *7*, 11921−11929.

(11) Yang, J.; Kim, S.; Choi, W.; Park, S. H.; Jung, Y.; Cho, M.-H.; Kim, H. Improved Growth Behavior of Atomic-Layer-Deposited High-k Dielectrics on Multilayer MoS2 by Oxygen Plasma Pretreatment. *ACS Appl. Mater. Interfaces* **2013**, *5*, 4739−4744.

(12) Azcatl, A.; McDonnell, S.; Santosh, K. C.; Peng, X.; Dong, H.; Qin, X.; Addou, R.; Mordi, G. I.; Lu, N.; Kim, J.; Kim, M. J.; Cho, K.; Wallace, R. M. MoS_2 Functionalization for Ultra-Thin Atomic Layer Deposited Dielectrics. *Appl. Phys. Lett.* **2014**, *104*, 111601.

(13) Azcatl, A.; Santosh, K. C.; Peng, X.; Lu, N.; McDonnell, S.; Qin, X.; de Dios, F.; Addou, R.; Kim, J.; Kim, M. J.; Cho, K.; Wallace, R. M. HfO_2 on UV−O_3 exposed Transition Metal Dichalcogenides: Interfacial Reactions Study. *2D Mater.* **2015**, *2*, 014004.

(14) Wirtz, C.; Hallam, T.; Cullen, C. P.; Berner, N. C.; O'Brien, M.; Marcia, M.; Hirsch, A.; Duesberg, G. S. Atomic Layer Deposition on 2D Transition Metal Chalcogenides: Layer Dependent Reactivity and Seeding with Organic Ad-Layers. *Chem. Commun.* **2015**, *51*, 16553−16556.

(15) Son, S.; Yu, S.; Choi, M.; Kim, D.; Choi, C. Improved High Temperature Integration of Al_2O_3 on MoS_2 by Using a Metal Oxide Buffer Layer. *Appl. Phys. Lett.* **2015**, *106*, No. 021601.

(16) Qian, Q.; Li, B.; Hua, M.; Zhang, Z.; Lan, F.; Xu, Y.; Yan, R.; Chen, K. J. Improved Gate Dielectric Deposition and Enhanced Electrical Stability for Single-Layer MoS2 MOSFET with an AlN Interfacial Layer. *Sci. Rep.* **2016**, *6*, 27676.

(17) Qian, Q.; Zhang, Z.; Hua, M.; Tang, G.; Lei, J.; Lan, F.; Xu, Y.; Yan, R.; Chen, K. J. Enhanced Dielectric Deposition on Single-Layer MoS_2 with Low Damage Using Remote N_2 Plasma Treatment. *Nanotechnology* **2017**, *28*, 175202.

(18) Zhang, H.; Arutchelvan, G.; Meersschaut, J.; Gaur, A.; Conard, T.; Bender, H.; Lin, D.; Asselberghs, I.; Heyns, M.; Radu, I.; Vandervorst, W.; Delabie, A. MoS_2 Functionalization with a Sub-Nm Thin SiO_2 Layer for Atomic Layer Deposition of High-κ Dielectrics. *Chem. Mater.* **2017**, *29*, 6772−6780.

(19) Kropp, J. A.; Cai, Y.; Yao, Z.; Zhu, W.; Gougousi, T. Atomic Layer Deposition of Al_2O_3 and TiO_2 on MoS_2 Surfaces. *J. Vac. Sci. Technol., A* **2018**, *36*, No. 06A101.
(20) Wiegenstein, C. G.; Schulz, K. H. Methanethiol Adsorption on Defective MoS2(0001) Surfaces. *J. Phys. Chem. B* **1999**, *103*, 6913−6918.
(21) Bertolazzi, S.; Bonacchi, S.; Nan, G.; Pershin, A.; Beljonne, D.; Samorì, P. Engineering Chemically Active Defects in Monolayer MoS_2 Transistors via Ion-Beam Irradiation and Their Healing via Vapor Deposition of Alkanethiols. *Adv. Mater.* **2017**, *29*, 1606760.
(22) Ma, Q.; Odenthal, P. M.; Mann, J.; Le, D.; Wang, C. S.; Zhu, Y.; Chen, T.; Sun, D.; Yamaguchi, K.; Tran, T.; Wurch, M.; McKinley, J. L.; Wyrick, J.; Magnone, K.; Heinz, T. F.; Rahman, T. S.; Kawakami, R.; Bartels, L. Controlled Argon Beam-Induced Desulfurization of Monolayer Molybdenum Disulfide. *J. Phys. Condens. Matter* **2013**, *25*, 252201.
(23) Makarova, M.; Okawa, Y.; Aono, M. Selective Adsorption of Thiol Molecules at Sulfur Vacancies on MoS_2(0001), Followed by Vacancy Repair via S−C Dissociation. *J. Phys. Chem. C* **2012**, *116*, 22411−22416.
(24) Kim, J.-S.; Yoo, H.-W.; Choi, H. O.; Jung, H.-T. Tunable Volatile Organic Compounds Sensor by Using Thiolated Ligand Conjugation on MoS_2. *Nano Lett.* **2014**, *14*, 5941−5947.
(25) Nguyen, E. P.; Carey, B. J.; Ou, J. Z.; van Embden, J.; Gaspera, E. D.; Chrimes, A. F.; Spencer, M. J. S.; Zhuiykov, S.; Kalantar-zadeh, K.; Daeneke, T. Electronic Tuning of 2D MoS_2 through Surface Functionalization. *Adv. Mater.* **2015**, *27*, 6225−6229.
(26) Sim, D. M.; Kim, M.; Yim, S.; Choi, M.-J.; Choi, J.; Yoo, S.; Jung, Y. S. Controlled Doping of Vacancy-Containing Few-Layer MoS_2 via Highly Stable Thiol-Based Molecular Chemisorption. *ACS Nano* **2015**, *9*, 12115−12123.
(27) Cho, K.; Min, M.; Kim, T.-Y.; Jeong, H.; Pak, J.; Kim, J.-K.; Jang, J.; Yun, S. J.; Lee, Y. H.; Hong, W.-K.; Lee, T. Electrical and Optical Characterization of MoS2 with Sulfur Vacancy Passivation by Treatment with Alkanethiol Molecules. *ACS Nano* **2015**, *9*, 8044−8053.
(28) Chen, X.; Berner, N. C.; Backes, C.; Duesberg, G. S.; McDonald, A. R. Functionalization of Two-Dimensional MoS2: On the Reaction Between MoS2 and Organic Thiols. *Angew. Chem., Int. Ed.* **2016**, *55*, 5803−5808.
(29) Li, Q.; Zhao, Y.; Ling, C.; Yuan, S.; Chen, Q.; Wang, J. Towards a Comprehensive Understanding of the Reaction Mechanisms Between Defective MoS_2 and Thiol Molecules. *Angew. Chem., Int. Ed.* **2017**, *56*, 10501−10505.
(30) Förster, A.; Gemming, S.; Seifert, G.; Tománek, D. Chemical and Electronic Repair Mechanism of Defects in MoS_2 Monolayers. *ACS Nano* **2017**, *11*, 9989−9996.
(31) Förster, A.; Gemming, S.; Seifert, G. Functional Thiols as Repair and Doping Agents of Defective MoS_2 Monolayers. *J. Phys. Condens. Matter* **2018**, *30*, 235302.
(32) Gul, A.; Bacaksiz, C.; Unsal, E.; Akbali, B.; Tomak, A.; Zareie, H. M.; Sahin, H. Theoretical and Experimental Investigation of Conjugation of 1,6-Hexanedithiol on MoS2. *Mater. Res. Express* **2018**, *5*, No. 036415.
(33) Chen, X.; McGlynn, C.; McDonald, A. R. Two-Dimensional MoS_2 Catalyzed Oxidation of Organic Thiols. *Chem. Mater.* **2018**, *30*, 6978−6982.
(34) Cho, K.; Pak, J.; Kim, J.-K.; Kang, K.; Kim, T.-Y.; Shin, J.; Choi, B. Y.; Chung, S.; Lee, T. Contact-Engineered Electrical Properties of MoS_2 Field-Effect Transistors via Selectively Deposited Thiol-Molecules. *Adv. Mater.* **2018**, *30*, 1705540.
(35) Zhu, J.; Wang, Z.; Yu, H.; Li, N.; Zhang, J.; Meng, J.; Liao, M.; Zhao, J.; Lu, X.; Du, L.; Yang, R.; Shi, D.; Jiang, Y.; Zhang, G. Argon Plasma Induced Phase Transition in Monolayer MoS2. *J. Am. Chem. Soc.* **2017**, *139*, 10216−10219.
(36) Spychalski, W. L.; Pisarek, M.; Szoszkiewicz, R. Microscale Insight into Oxidation of Single MoS_2 Crystals in Air. *J. Phys. Chem. C* **2017**, *121*, 26027−26033.
(37) Provine, J.; Schindler, P.; Torgersen, J.; Kim, H. J.; Karnthaler, H.-P.; Prinz, F. B. Atomic Layer Deposition by Reaction of Molecular Oxygen with Tetrakisdimethylamido-Metal Precursors. *J. Vac. Sci. Technol., A* **2015**, *34*, 01A138.
(38) Xie, Q.; Jiang, Y.-L.; Detavernier, C.; Deduytsche, D.; Van Meirhaeghe, R. L.; Ru, G.-P.; Li, B.-Z.; Qu, X.-P. Atomic Layer Deposition of TiO2 from Tetrakis-Dimethyl-Amido Titanium or Ti Isopropoxide Precursors and H2O. *J. Appl. Phys.* **2007**, *102*, No. 083521.
(39) Ataca, C.; Ciraci, S. Dissociation of H_2O at the Vacancies of Single-Layer MoS_2. *Phys. Rev. B* **2012**, *85*, 195410.
(40) González, C.; Biel, B.; Dappe, Y. J. Adsorption of Small Inorganic Molecules on a Defective MoS_2 Monolayer. *Phys. Chem. Chem. Phys.* **2017**, *19*, 9485−9499.
(41) Liu, Y.; Stradins, P.; Wei, S.-H. Air Passivation of Chalcogen Vacancies in Two-Dimensional Semiconductors. *Angew. Chem., Int. Ed.* **2016**, *55*, 965−968.
(42) Li, H.; Huang, M.; Cao, G. Markedly Different Adsorption Behaviors of Gas Molecules on Defective Monolayer MoS2: A First-Principles Study. *Phys. Chem. Chem. Phys.* **2016**, *18*, 15110−15117.
(43) Liu, H.; Han, N.; Zhao, J. Atomistic Insight into the Oxidation of Monolayer Transition Metal Dichalcogenides: From Structures to Electronic Properties. *RSC Adv.* **2015**, *5*, 17572−17581.
(44) Kc, S.; Longo, R. C.; Wallace, R. M.; Cho, K. Surface Oxidation Energetics and Kinetics on MoS_2 Monolayer. *J. Appl. Phys.* **2015**, *117*, 135301.
(45) Lin, X.; Ni, J. Charge and Magnetic States of Mn-, Fe-, and Co-Doped Monolayer MoS2. *J. Appl. Phys.* **2014**, *116*, No. 044311.
(46) Wu, M.; Yao, X.; Hao, Y.; Dong, H.; Cheng, Y.; Liu, H.; Lu, F.; Wang, W.; Cho, K.; Wang, W.-H. Electronic Structures, Magnetic Properties and Band Alignments of 3d Transition Metal Atoms Doped Monolayer MoS2. *Phys. Lett. A* **2018**, *382*, 111−115.
(47) Tongay, S.; Suh, J.; Ataca, C.; Fan, W.; Luce, A.; Kang, J. S.; Liu, J.; Ko, C.; Raghunathanan, R.; Zhou, J.; Ogletree, F.; Li, J.; Grossman, J. C.; Wu, J. Defects Activated Photoluminescence in Two-Dimensional Semiconductors: Interplay between Bound, Charged, and Free Excitons. *Sci. Rep.* **2013**, *3*, 2657.
(48) Wei, X.; Yu, Z.; Hu, F.; Cheng, Y.; Yu, L.; Wang, X.; Xiao, M.; Wang, J.; Wang, X.; Shi, Y. Mo-O Bond Doping and Related-Defect Assisted Enhancement of Photoluminescence in Monolayer MoS2. *AIP Adv.* **2014**, *4*, 123004.
(49) Qi, L.; Wang, Y.; Shen, L.; Wu, Y. Chemisorption-Induced *n*-Doping of MoS_2 by Oxygen. *Appl. Phys. Lett.* **2016**, *108*, No. 063103.
(50) Lu, H.; Kummel, A.; Robertson, J. Passivating the Sulfur Vacancy in Monolayer MoS_2. *APL Mater.* **2018**, *6*, No. 066104.
(51) Akdim, B.; Pachter, R.; Mou, S. Theoretical Analysis of the Combined Effects of Sulfur Vacancies and Analyte Adsorption on the Electronic Properties of Single-Layer MoS2. *Nanotechnology* **2016**, *27*, 185701.
(52) Rao, R.; Islam, A. E.; Campbell, P. M.; Vogel, E. M.; Maruyama, B. In Situthermal Oxidation Kinetics in Few Layer MoS2. *2D Mater.* **2017**, *4*, 025058.
(53) Huo, N.; Yang, Y.; Wu, Y.-N.; Zhang, X.-G.; Pantelides, S. T.; Konstantatos, G. High Carrier Mobility in Monolayer CVD-Grown MoS_2 through Phonon Suppression. *Nanoscale* **2018**, *10*, 15071−15077.
(54) Singh, A. K.; Hennig, R. G.; Davydov, A. V.; Tavazza, F. Al_2O_3 as a Suitable Substrate and a Dielectric Layer for *N*-Layer MoS_2. *Appl. Phys. Lett.* **2015**, *107*, No. 053106.
(55) Kufer, D.; Konstantatos, G. Highly Sensitive, Encapsulated MoS2 Photodetector with Gate Controllable Gain and Speed. *Nano Lett.* **2015**, *15*, 7307−7313.
(56) Price, K. M.; Najmaei, S.; Ekuma, C. E.; Burke, R. A.; Dubey, M.; Franklin, A. D. Plasma-Enhanced Atomic Layer Deposition of HfO_2 on Monolayer, Bilayer, and Trilayer MoS_2 for the Integration of High-κ Dielectrics in Two-Dimensional Devices. *ACS Appl. Nano Mater.* **2019**, *2*, 4085−4094.
(57) Henegar, D. A. J.; Gougousi, P. T. Comparison of the Reactivity of Alkyl and Alkyl Amine Precursors with Native Oxide

https://dx.doi.org/10.1021/acsami.0c13095
ACS Appl. Mater. Interfaces 2020, 12, 48150−48160

GaAs(100) and InAs(100) Surfaces. *Appl. Surf. Sci.* **2016**, *390*, 870−881.
(58) Horcas, I.; Fernández, R.; Gómez-Rodríguez, J. M.; Colchero, J.; Gómez-Herrero, J.; Baro, A. M. WSXM: A Software for Scanning Probe Microscopy and a Tool for Nanotechnology. *Rev. Sci. Instrum.* **2007**, *78*, No. 013705.
(59) Kresse, G.; Furthmüller, J. Efficient Iterative Schemes for Ab Initio Total-Energy Calculations Using a Plane-Wave Basis Set. *Phys. Rev. B* **1996**, *54*, 11169−11186.
(60) Perdew, J. P.; Burke, K.; Ernzerhof, M. Generalized Gradient Approximation Made Simple. *Phys. Rev. Lett.* **1996**, *77*, 3865−3868.
(61) Nosé, S. A Unified Formulation of the Constant Temperature Molecular Dynamics Methods. *J. Chem. Phys.* **1984**, *81*, 511−519.
(62) Hoover, W. G. Canonical Dynamics: Equilibrium Phase-Space Distributions. *Phys. Rev. A* **1985**, *31*, 1695−1697.
(63) van de Walle, A.; Asta, M.; Ceder, G. The Alloy Theoretic Automated Toolkit: A User Guide. *Calphad* **2002**, *26*, 539−553.

https://dx.doi.org/10.1021/acsami.0c13095
ACS Appl. Mater. Interfaces 2020, 12, 48150−48160